



1 Simultaneous Measurement of Urban and Rural Particles in Beijing, Part II: Case Studies  
2 of Haze Events and Regional Transport

3 Yang Chen,<sup>1</sup> Guangming Shi,<sup>1,3</sup> Jing Cai,<sup>2</sup> Zongbo Shi,<sup>4,5</sup> Zhichao Wang,<sup>1</sup> Xiaojiang Yao,<sup>1</sup>  
4 Mi Tian,<sup>1</sup> Chao Peng,<sup>1</sup> Yiqun Han,<sup>2</sup> Tong Zhu,<sup>2</sup> Yue Liu,<sup>2</sup> Xi Yang,<sup>2</sup> Mei Zheng,<sup>2\*</sup> Fumo  
5 Yang,<sup>1,3\*</sup> and Kebin He<sup>6</sup>

6 <sup>1</sup>Chongqing Institute of Green and Intelligent Technology, Chinese Academy of Sciences,  
7 Chongqing 400714, China

8 <sup>2</sup>SKL-ESPC and BIC-ESAT, College of Environmental Sciences and Engineering, Peking  
9 University, Beijing 100871, China

10 <sup>3</sup> Department of Environmental Science and Engineering, College of Architecture and  
11 Environment, Sichuan University, Chengdu 610065, China

12 <sup>4</sup> School of Geography, Earth and Environmental Sciences, the University of Birmingham,  
13 Birmingham B15 2TT, UK

14 <sup>5</sup> Institute of Surface-Earth System Science, Tianjin University, Tianjin 300072, China

15 <sup>6</sup> School of Environment, Tsinghua University, Beijing 100084, China

16 Corresponding to Fumo Yang (fmyang@scu.edu.cn) and Mei Zheng  
17 (mzheng@pku.edu.cn)



18 Abstract

19 Two parallel field studies were conducted simultaneously at both urban and rural sites in  
20 Beijing from 11/01/2016 to 11/29/2016. Online single-particle chemical composition  
21 analysis was used as a tracer system to investigate the impact of heating activities and  
22 formation of haze events. Central heating elevated EC-Nit, EC-Nit-Sul, and ECOC-Nit  
23 levels by 1.5–2.0 times due to the increased use of coal in the urban areas. However, in the  
24 rural areas, residential heating which mainly consumes low-quality coal and biomass  
25 burning elevated ECOC-Nit-Sul, Nak-Nit, and OC-Sul levels by 1.2–1.5 times. Four severe  
26 haze events (hourly  $PM_{2.5} > 200 \mu g m^{-3}$ ) occurred at both sites during the studies. In each  
27 event, a pattern of “transport and accumulation” was found. In the first stage, particles were  
28 regionally transported from the south or southwest and accumulated under air stagnations,  
29 creating significant secondary formation. Consequently, the boosting of  $PM_{2.5}$  led to severe  
30 haze. At both sites, the severe haze occurred due to different patterns of local emission,  
31 transport, and secondary processes. At PG, the sulfate-rich residential coal burning  
32 particles were dominant. The regional transport between PG and PKU was simulated using  
33 the WRF-HYSPLIT model, confirming that the transport from PG to PKU was significant,  
34 but PKU to PG occurred occasionally. These cases can explain the serious air pollution in  
35 the urban areas of Beijing and the interaction between urban and rural areas. This study  
36 can provide references for enhancing our understanding of haze formation in Beijing.

37 Keywords: urban; regional; single particle; transport; pollution event

38



## 39 **1. Introduction**

40 The Beijing-Tianjin-Hebei (BTH) area in China has been suffering from extreme haze  
41 events caused by high concentrations of  $\text{PM}_{2.5}$  ( $> 200 \mu\text{g m}^{-3}$ ) since 2013 (Guo et al., 2014).  
42 Studies have been performed to understand the formation of such massive haze events in  
43 Beijing (Tian et al., 2014; Quan et al., 2013; Che et al., 2014; He et al., 2015). Traffic,  
44 cooking, and coal combustion emissions accounted for 41–59% of the total submicron  
45 organic aerosols, and the remainder were secondary organic aerosols (Sun et al., 2014).  
46 Model studies suggest that temperature inversion, low boundary layer, and transported  
47 pollutants cause the local accumulation of  $\text{PM}_{2.5}$  in urban areas (Zhang et al., 2015). In  
48 short, significant local emissions, unfavorable meteorological conditions, and regional  
49 transport play essential roles in accumulating  $\text{PM}_{2.5}$ .

50 There are unresolved issues surrounding whether the rapid boosting of PM in Beijing is  
51 due to local secondary aerosol formation or transport. Wang et al. (2016) have proposed  
52 that the accumulation of nitrates is dominant at the beginning of haze events, and then  
53 sulfate increases because  $\text{SO}_2$  is oxidized into sulfate in ammonium-rich conditions.  
54 Moreover, Cheng et al. (2016) have suggested that  $\text{NO}_2$  could oxidize  $\text{SO}_2$  to sulfate on the  
55 surface of alkali aerosols. However, Li et al. (2015) have argued that regionally transported  
56  $\text{PM}_{2.5}$  is a significant cause of severe haze. Last but not least, Sun et al. (2014); Sun et al.  
57 (2013a) have proposed that both local formation and regional transport are factors. Except  
58 for model studies, most field studies have focused on urban areas in Beijing, with limited  
59 attention to rural areas. The characterization of rural PM is also essential to understanding  
60 the evolution of particulate haze events.



61 The cold winter results in the necessity of heating, consequently impacting the air quality  
62 in BTH (Sun et al., 2014). In urban areas, central heating systems use coal or natural gas,  
63 while rural households use coal or biofuel for heating and cooking. Residential emissions  
64 in Beijing reach about 4 million tons, mainly caused by low-efficiency coal combustion  
65 (Li et al., 2015). Coal combustion organic aerosols (CCOA) account for 20–32% of total  
66 submicron OA in Beijing (Sun et al., 2014; Sun et al., 2013a). However, whether CCOA  
67 is contributed by central or household heating remains unclear. Notably, central and  
68 household heating release distinct particles due to different burning conditions (Lee et al.,  
69 2005; Chagger et al., 1999). Therefore, analyzing household heating and cooking emissions  
70 in rural areas is also beneficial for understanding the source of urban PM<sub>2.5</sub> in Beijing.

71 As mentioned in Part I (Chen et al., 2020), two SPAMSSs were deployed simultaneously in  
72 Peking University (PKU) and Pinggu (PG) in order to monitor urban and rural particles in  
73 the Beijing region. In Part II, the detailed analysis of haze events, effects of heating  
74 activities, and evidence of regional transport between urban and rural areas are addressed.

## 75 **2. Methodology**

### 76 **2.1 Sampling sites, instrumentation, and data analysis**

77 Please refer to Part I and Support Information for the detail (Chen et al., 2020). Briefly, the  
78 field studies were performed simultaneously at PKU (116.32°E, 39.99°N) and PG (117.05  
79 °E, 40.17°N) from 11/01/2016 to 11/29/2016. The two sites represent both typical urban  
80 and rural areas, respectively. The local meteorological data is retrieved from the local  
81 meteorological offices. Two SPAMSSs (0515, Hexin Inc., Guangzhou, China) were



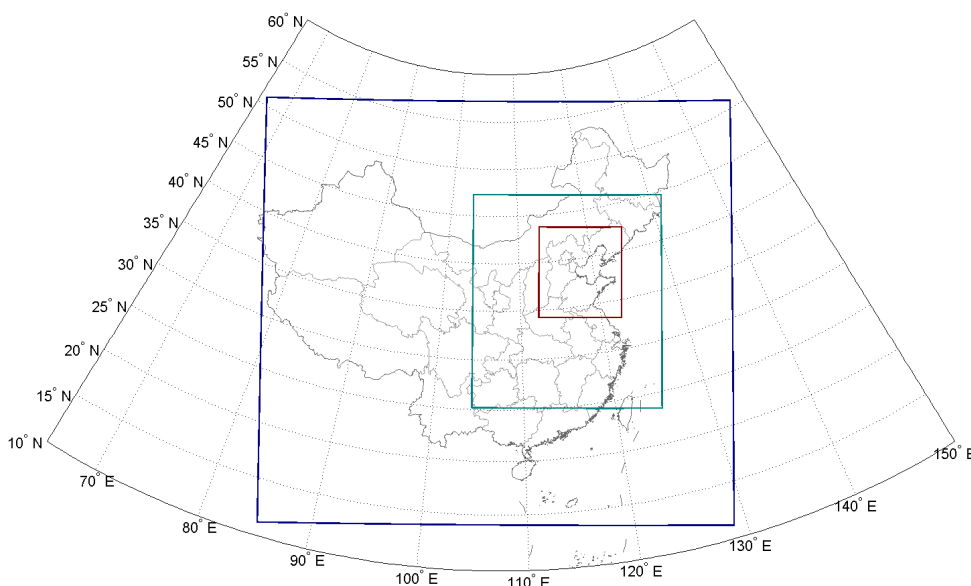
82 deployed at both sites for parallel measurements. SPAMS generates single particle mass  
83 spectra from the captured individual particles. The technical description of SPAMS is  
84 available in the literature (Li et al., 2011). A neural network algorithm based on adaptive  
85 resonance theory (ART-2a) was applied for clustering particle types in the datasets (Song  
86 et al., 1999). During the clustering procedure, the relative peak areas (RPA) of sulfate and  
87 nitrate are considered. A criterion of RPA >0.1 is used to identify the nitrate-rich (-Nit),  
88 sulfate-rich (-Sul), or both. Based on the strategy, 20 and 19 particle types were identified  
89 at PKU and PG respectively.

## 90 **2.2 Dispersion model**

91 A WRF-HYSPLIT (Weather Research and Forecasting - Hybrid Single Particle  
92 Lagrangian Integrated Trajectory) coupling model was used to describe the air parcel  
93 movement between PKU and PG. The description of the model is available at  
94 <https://www.arl.noaa.gov/hysplit/inline-wrf-hysplit-coupling/>. The HYSPLIT dispersion  
95 simulations were driven by the meteorological data fields from the WRF model version  
96 3.8. The WRF domains are shown in Figure 2. The innermost domain was configured to  
97 cover northern China with a horizontal resolution of 3 km and 35 vertical layers. The  
98 longwave and shortwave radiation schemes were set as the RRTMG and Dudhia scheme  
99 respectively. The Yonsei University (YSU) scheme was used for the PBL parameterization.  
100 For the microphysics, the Morrison 2-moment scheme was adopted. NCEP FNL (National  
101 Centers for Environmental Prediction, final) data with a resolution of  $1^{\circ} \times 1^{\circ}$  was employed  
102 as initial and boundary conditions. The WRF simulation was initialized as a “cold start” at  
103 0000 UTC each day and ran for 36 hours. The first 12 hours were discarded as model spin-



104 up time, and the output for the following 24 hours was retained. This process was repeated  
105 to produce continuous meteorological data fields for the whole experimental period. The  
106 HYSPLIT was set to release 10,000 Lagrangian particles within one hour at PKU and PG,  
107 10 m above ground level. The concentration of released particles was simulated with one  
108 vertical layer extending from 0 to 1,000 m above ground level.



109

110 Figure 1. Spatial configuration of domains used for WRF simulation.

### 111 3. Results and discussion

#### 112 3.1 Particle type description

113 Particle types, their ratios at both sites, and major chemical composition are shown in Table  
114 1. The typical single-particle mass spectra of each particle type are available in Supportive  
115 Information and (Chen et al., 2020).



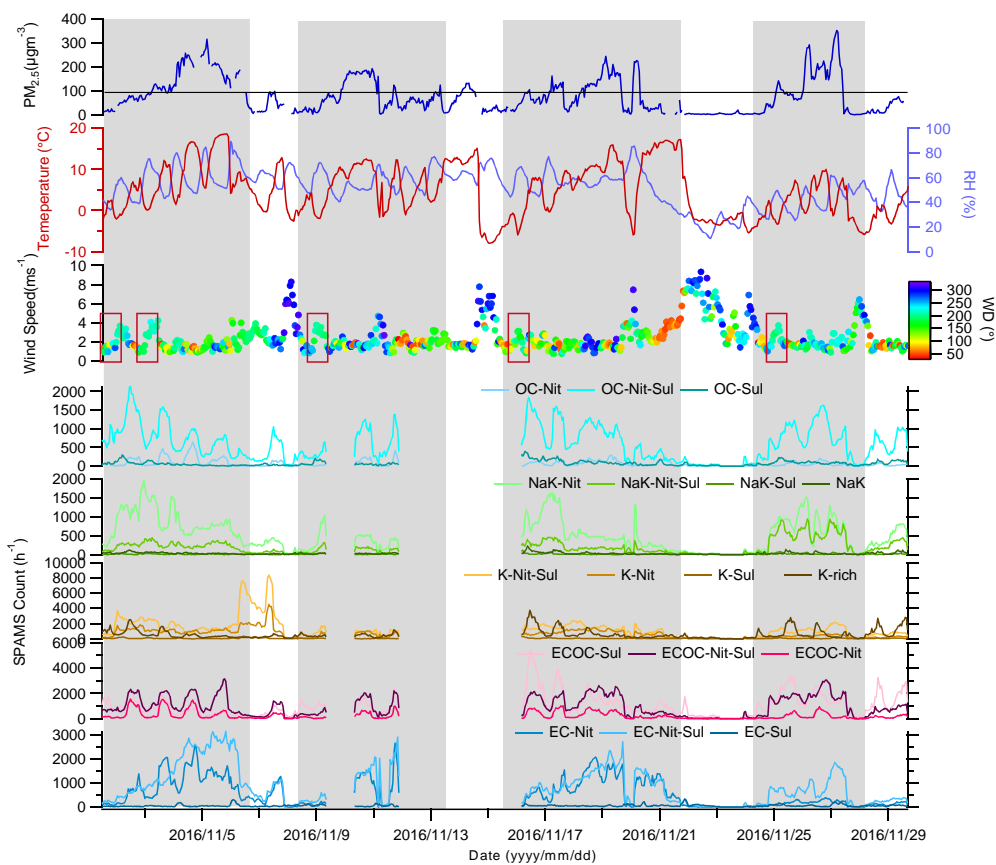
116 Table 1. Particle types and their relative ratios and chemical composition

	Both	PKU	PG	Chemical Composition*
EC	EC-Nit	7.0	2.0	$C_n^+$ , $C_n^-$ , $HSO_4^-$ , $NO_2^-$ ,
	EC-Nit-Sul	10.5	3.5	$NO_3^-$
	EC-Sul	0.7	0.1	
ECOC	ECOC-Nit-Sul	12.0	18.6	$C_n^+$ , $C_n^-$ , $C_xH_y^+$ , $C_xH_yO_z^+$
	ECOC-Sul	12.7	9.8	$HSO_4^-$ , $NO_3^-$
K-rich	K-rich	7.2	6.4	$K^+$ , $NH_4^+$ , $HSO_4^-$ , $NO_3^-$
	K-Nit	8.0	8.2	$NO_2^-$
	K-Nit-Sul	16.0	1.9	
	K-Sul	0.6	4.5	
NaK	NaK	0.4	1.8	$Na^+$ , $K^+$ , $NH_4^+$ , $HSO_4^-$ ,
	NaK-Nit	6.4	1.7	$NO_3^-$
	NaK-Nit-Sul	2.5	1.9	
	NaK-Sul	0.2	0.4	
OC	OC-Nit-Sul	7.4	21.3	$C_xH_y^+$ , $C_xH_yO_z^+$ , $NH_4^+$
	OC-Sul	0.9	6.9	$HSO_4^-$ , $NO_3^-$
	Ca-dust	0.4	0.1	$Cl^-$
Fe	Fe-rich	3.1	1.8	$Fe^+$ , Org, $HSO_4^-$ , $NO_3^-$
	ECOC-Nit	3.1%		
	OC-Nit	0.9%		
	K-Amine-Nit-Sul	0.1%		TMA, $NH_4^+$ , $HSO_4^-$ , $NO_3^-$
	ECOC		5.9%	$C_n^+$ , $C_n^-$ , $C_xH_y^+$ , $C_xH_yO_z$
	OC		3.3%	$C_xH_y^+$ , $C_xH_yO_z$

117 \* chemical species with relative peak area >0.1

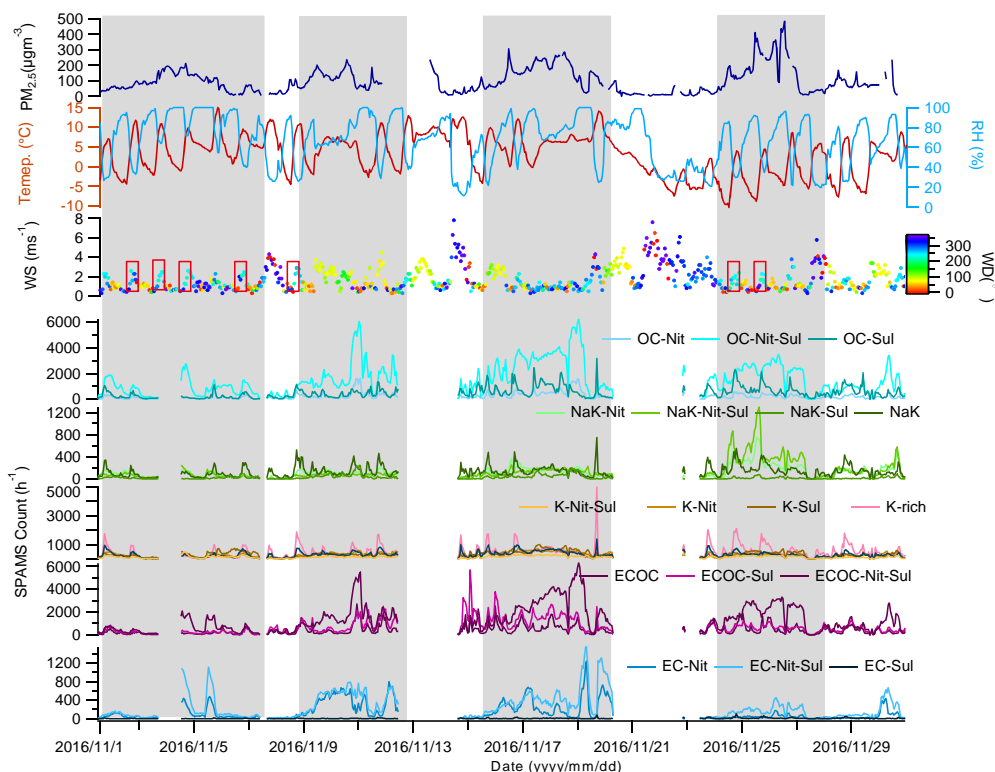
### 118 3.2 Overview of haze events

119 Figures 2 and 3 show the overview of  $PM_{2.5}$ , meteorology parameters, and time trends of  
 120 particles at PKU and PG respectively. There were four parallel haze events during the  
 121 observation period: 11/01/2016–11/07/2016 (E1), 11/09/2016–11/15/2016 (E2),  
 122 11/15/2016–11/22/2016 (E3), and 11/25/2016–11/28/2016 (E4).



123

124 Figure 2. Time trends of  $PM_{2.5}$ , temperature, relative humidity, wind direction, wind speed,  
125 and single particle types at PKU. The rectangles indicate the transport of regional particles.



126

127 Figure 3. Time trends of PM<sub>2.5</sub>, temperature, relative humidity, wind direction, wind speed,  
128 and single particle types at PG. The rectangles indicate the transport of regional particles.

129 The pattern of single-particle chemical composition, represented by normalized number  
130 fractions of particle types in different periods, is used to describe PM characteristics. The  
131 correlations of normalized number fractions during events at PKU and PG are shown in  
132 Tables 1 and S3. E1\_PKU was well correlated with Clear1 ( $R = 0.90$ ) and E2\_PKU ( $R =$   
133  $0.86$ ), but poorly correlated with Clear2 ( $R = 0.38$ ) and E4 ( $R = 0.64$ ). This is because  
134 E1\_PKU and E2\_PKU occurred before the heating period, but E4\_PKU occurred after  
135 (11/15/2016). The chemical compositions of the four events at PG are highly correlated



136 with each other (all  $R_s > 0.90$ , Table S3). These results indicate that the chemical  
137 composition patterns changed significantly at PKU, but insignificantly at PG.

138 Table 1. Correlations of number fractions of particle types in different events at PKU.

	E1	Clear1	E2	Clear2*	E4
E1	1				
Clear1	0.90	1			
E2	0.86	0.91	1		
Clear2	0.38	0.70	0.58	1	
E4	0.64	0.81	0.83	0.76	1

139 Note: The chemical composition of E3 is unavailable.

### 140 3.3 Influence of heating activities

141 Central heating began on 11/15/2016 in the urban area, while residential heating in the rural  
142 area had no distinct starting day. As such, the shift in emissions due to the increased use of  
143 solid fuel directly affected the particulate chemical composition. As shown in Figure 4, the  
144 normalized ratios of EC-Nit\_PKU, EC-Nit-Sul\_PKU, and OC-Nit\_PKU increased by  
145 about 1.5 times. EC-Nit\_PKU and EC-Nit-Sul\_PKU came from multiple local sources, one  
146 of which was coal burning in boilers (Xu et al., 2018b). In addition, high EC concentrations  
147 have been observed during the heating period each year for decades (Chen et al., 2016b).  
148 The mass spectra of OC-Nit particles were composed of a series of ion fragments of  
149 polycyclic aromatic hydrocarbons (PAHs). The results are consistent with organic aerosols  
150 from coal burning in AMS-related studies (Wang et al., 2019; Sun et al., 2013b).  
151 Additionally, PM<sub>2.5</sub>-bound PAHs increased by three times when the heating period began  
152 in Beijing (Zhang et al., 2017). The results also suggest the potential health risks of coal  
153 burning in wintertime in Beijing (Linak et al., 2007; Chen et al., 2013).



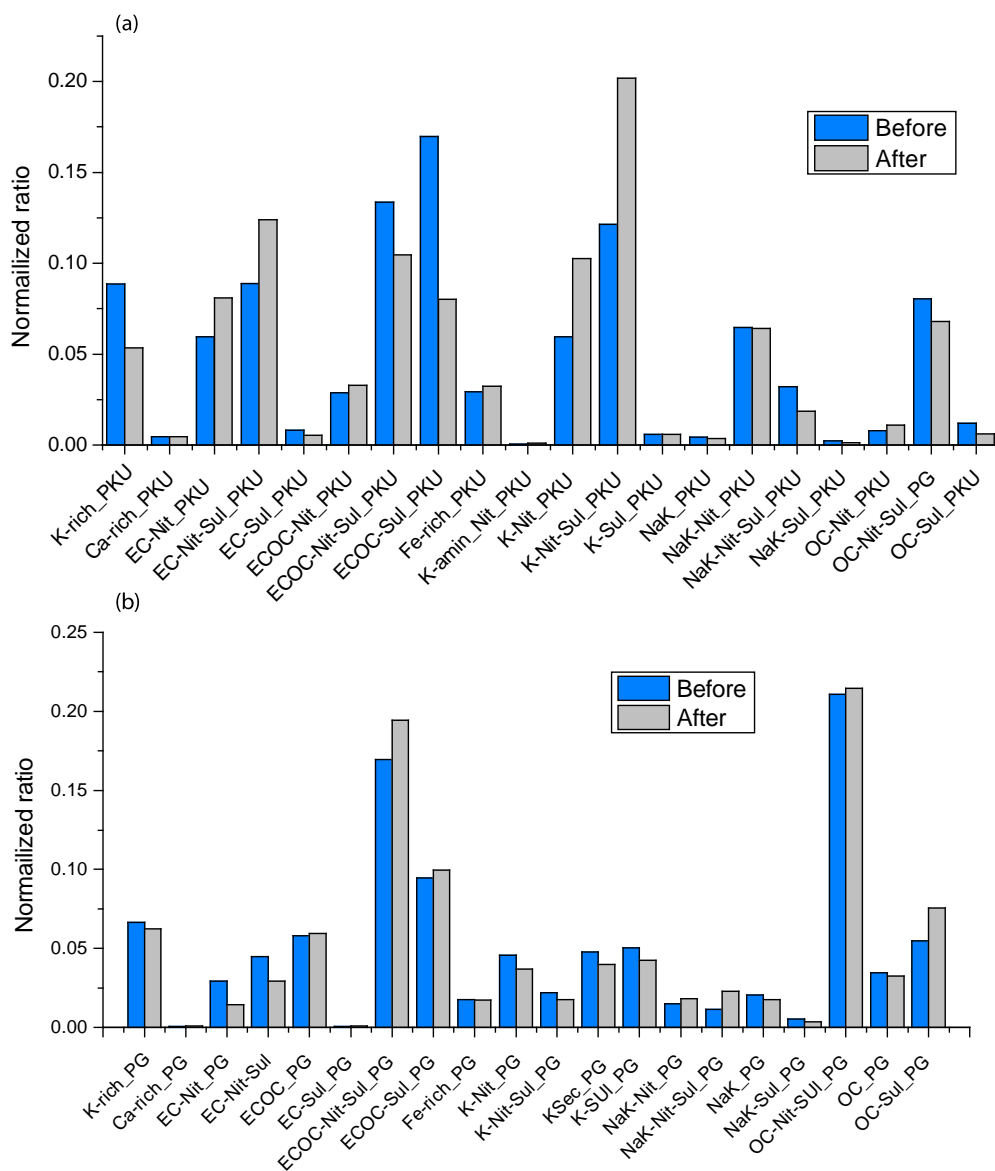
154 Biomass burning (BB) has been proven as a significant source of PM<sub>2.5</sub> in Beijing (Sun et  
155 al., 2013b; Sun et al., 2014), accounting for 9–12% (Liu et al., 2019). Anthropogenic BB,  
156 e.g. burning household biofuel, is prohibited in urban areas, but common in the areas  
157 surrounding Beijing. Most BB-related particles such as K-rich, K-Nit, and K-Nit-Sul at  
158 PKU were regional (Part I)(Chen et al., 2020). Not surprisingly, K-Nit\_PKU and K-Nit-  
159 Sul\_PKU both increased to 1.7 times after 11/15/2016. Interestingly, K-Amine-Nit\_PKU  
160 increased by 2.3 times after the heating period began, suggesting that BB is also a source  
161 of particulate amines in Beijing (Chen, 2019).

162 After 11/15/2016, NaK-Nit-Sul\_PG, Ca-rich\_PG, and OC-Sul\_PG increased by 1.96, 1.30,  
163 and 1.47 times respectively. As described above, in rural areas, low-quality coal is  
164 commonly used for heating and cooking, resulting in abundant EC-Sul, OC-Sul, and NaK-  
165 Nit-Sul (Xu et al., 2018a; Chen et al., 2016a). Interestingly, Ca-rich particles that were well  
166 correlated with OC-Sul ( $R = 0.79$ ) also increased, possibly due to flying ash from coal  
167 stoves.

168 A number of studies have reported contributions of coal burning to the submicron PM in  
169 urban areas of Beijing. According to these mass-based studies, PM-bound PAHs, chloride,  
170 sulfate, nitrate, and lead were markers from emissions of coal burning (Xu et al., 2018a;  
171 Sun et al., 2014; Ma et al., 2016; Zhang et al., 2019). Our result shows that these species  
172 were internally mixed as the ECOC particles. In particular, the household heating in PG  
173 released significant fractions of ECOC particles that arrived in the urban areas of Beijing.  
174 Likewise, K-rich particles from BB also transport to the urban areas of Beijing.



175 Conclusively, control of emissions from household emissions is also a key to improve the  
 176 air quality in Beijing



177

178 Figure 4. Variation of particle number ratio at PKU and PG before and after the heating  
 179 period 2017.



### 180 **3.4 Case studies: Haze events at PKU**

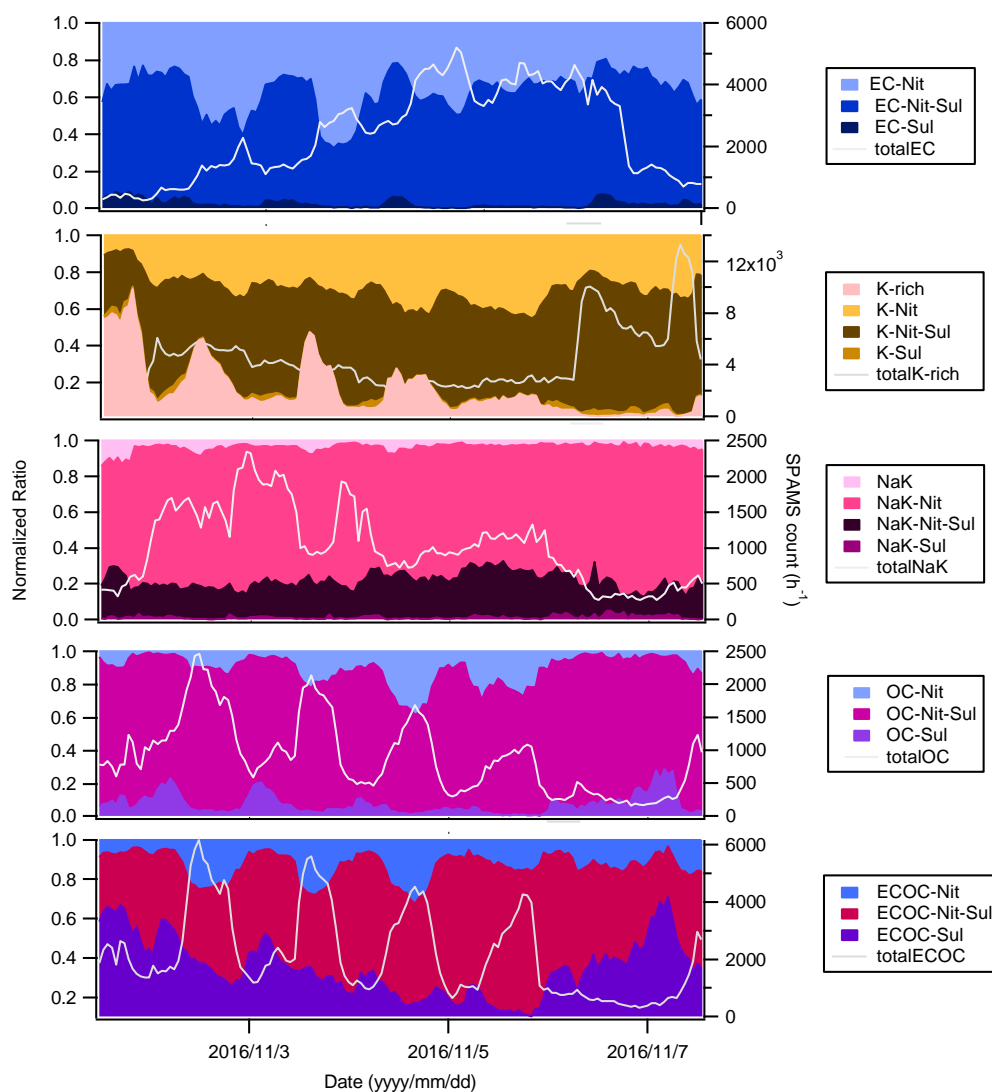
181 As shown in Figure 2, before  $\text{PM}_{2.5}$  increased to  $100 \mu\text{g m}^{-3}$  during E1\_PKU, two processes  
182 of  $\text{PM}_{2.5}$  transport were observed. The first process was from 12:00 on 11/01/2016 to 2:00  
183 on 11/02/2016, in which OC-Nit-Sul, K-Nit-Sul, K-Nit, NaK-Nit, K-Nit-Sul increased  
184 dramatically as the southern wind speed increased from  $1.3 \text{ m s}^{-1}$  to  $3.7 \text{ m s}^{-1}$ . The wind  
185 speed then decreased to  $1.2 \text{ m s}^{-1}$  until 16:00 on 11/02/2016, and the accumulation of  $\text{PM}_{2.5}$   
186 resulted in a concentration of  $67 \mu\text{g m}^{-3}$ . The second process occurred from 17:00 on  
187 11/02/2016 to 16:00 on 11/03/2016. Severe accumulation then started at 1:00 on  
188 11/04/2016, with an elevating trend of RH, reaching the highest  $\text{PM}_{2.5}$  level of  $314 \mu\text{g m}^{-3}$   
189 at 03:00 on 11/05/2016. After that, the wind dispersed the  $\text{PM}_{2.5}$  to  $11 \mu\text{g m}^{-3}$  at 17:00 on  
190 11/06/2016. In short, regional particles were transported from the south or southwest, then  
191 the accumulation of  $\text{PM}_{2.5}$  began. The accumulation of pollutants was accompanied by  
192 secondary aerosol formation, causing severe haze events.

193 During the events at PKU (Figure 2), particles transported from the south and southwest  
194 were observed and labeled with red rectangles. During E4\_PKU, the  $\text{PM}_{2.5}$  concentration  
195 increased from  $6 \mu\text{g m}^{-3}$  to  $122 \mu\text{g m}^{-3}$  between 15:00 on 11/24/2016 and 3:00 on  
196 11/25/2016 due to the southern wind, which brought abundant NaK-Nit, NaK-Nit-Sul,  
197 ECOC-Nit-Sul, and EC-Nit-Sul. Notably, regional particles were dramatically different  
198 from those of E1\_PKU due to the heating period. Then, under stagnant air conditions, the  
199 accumulation began at 22:00 on 11/25/2016 and lasted until 03:00 on 11/26/2016, with  
200  $\text{PM}_{2.5}$  levels reaching  $281 \mu\text{g m}^{-3}$ . At this stage, such local particles as OC-Nit-Sul, ECOC-  
201 Nit-Sul, and ECOC-Nit also showed accumulation and local emissions, while both the K-  
202 rich and NaK families showed a pattern of transport and accumulation (Figures 5 and 6).



203 As shown in Figure 5, which gives an integrated view of related particle types in urban  
204 Beijing, three types of particle evolution are distinguished during E1. First, EC particles,  
205 including EC-Nit, EC-Nit-Sul, and EC-Sul, show trends of accumulation, but with clear  
206 patterns of emissions, suggesting a pattern of emission and accumulation. Second, for  
207 regional particles such as the K-rich and NaK families, the processes of transport and  
208 accumulation were identified, with significant accumulation but unclear diurnal patterns.  
209 Third, the OC and ECOC families illustrated clear diurnal patterns of local emission and  
210 evolution. Notably, during the development of E1, the ratio of aged ECOC-Nit-Sul  
211 increased from 20% to 83%, suggesting that significant secondary processing occurred.

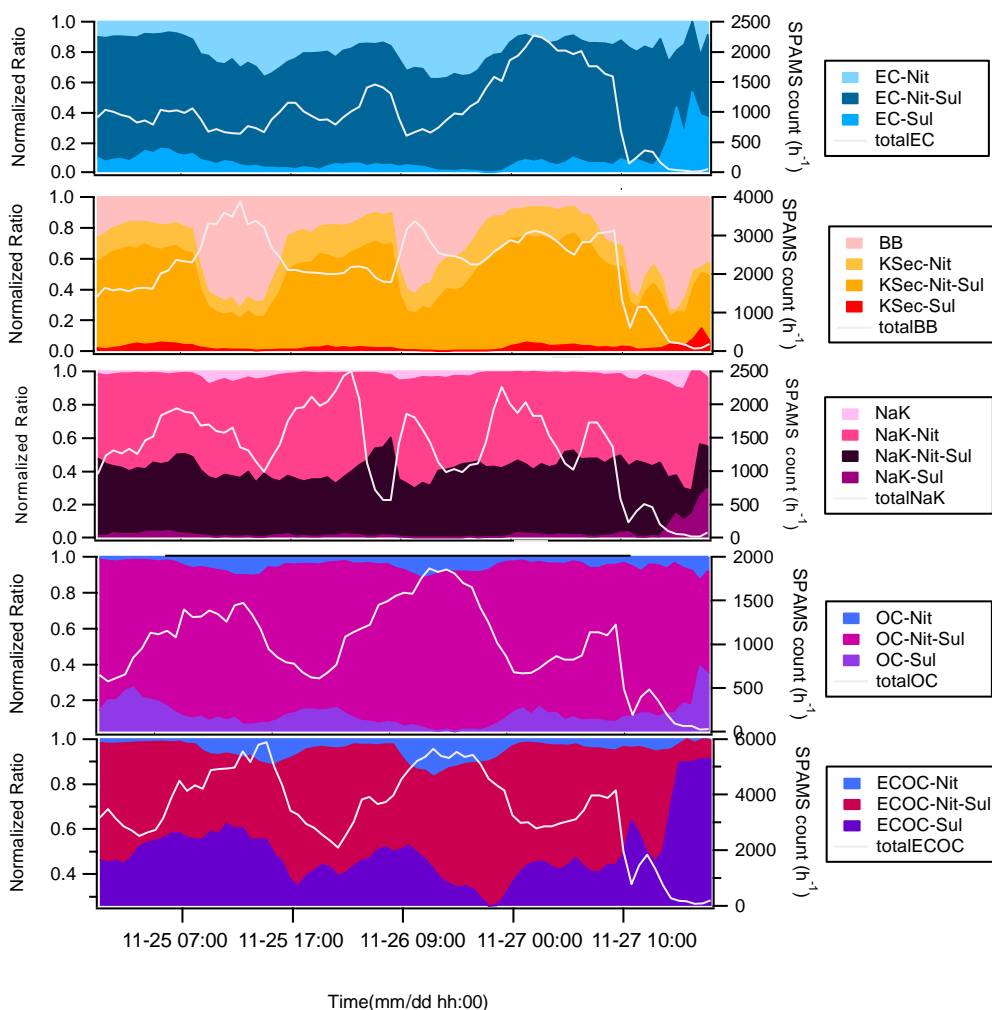
212 Due to the nature of SPAMS, the quantitative measurement of secondary formation is  
213 unavailable. Fortunately, as an integrated and extensive project, APHH-Beijing also  
214 included the online monitoring of the chemical composition of PM<sub>2.5</sub>. For example, during  
215 the transport stage of E4\_PKU, PM<sub>2.5</sub> was composed of 60% organic matter (OM) and 40%  
216 total nitrate, sulfate, and ammonium. During the accumulation stage, sulfate, nitrate, and  
217 ammonium levels were boosted up to 123  $\mu\text{g m}^{-3}$  (63%) together (Liu et al., 2019). Wang  
218 et al. (2019) also reported that, during the accumulation stage of E4\_PKU, the elevation of  
219 secondary OOA1 and OOA2 was significant.



220

221 Figure 5. Time trends of number ratios of particle types (left) and hourly counts of particle  
222 families (EC, BB, NaK, OC, and ECOC, right) during Pollution Event 1 (E1 11/01–11/08)  
223 at PKU.

224



225

226 Figure 6. Time trends of number ratios of particle types (left) and hourly counts of particle  
227 families (EC, BB, NaK, OC, and ECOC, right) during Pollution Event 4 (E4) at PKU.

228



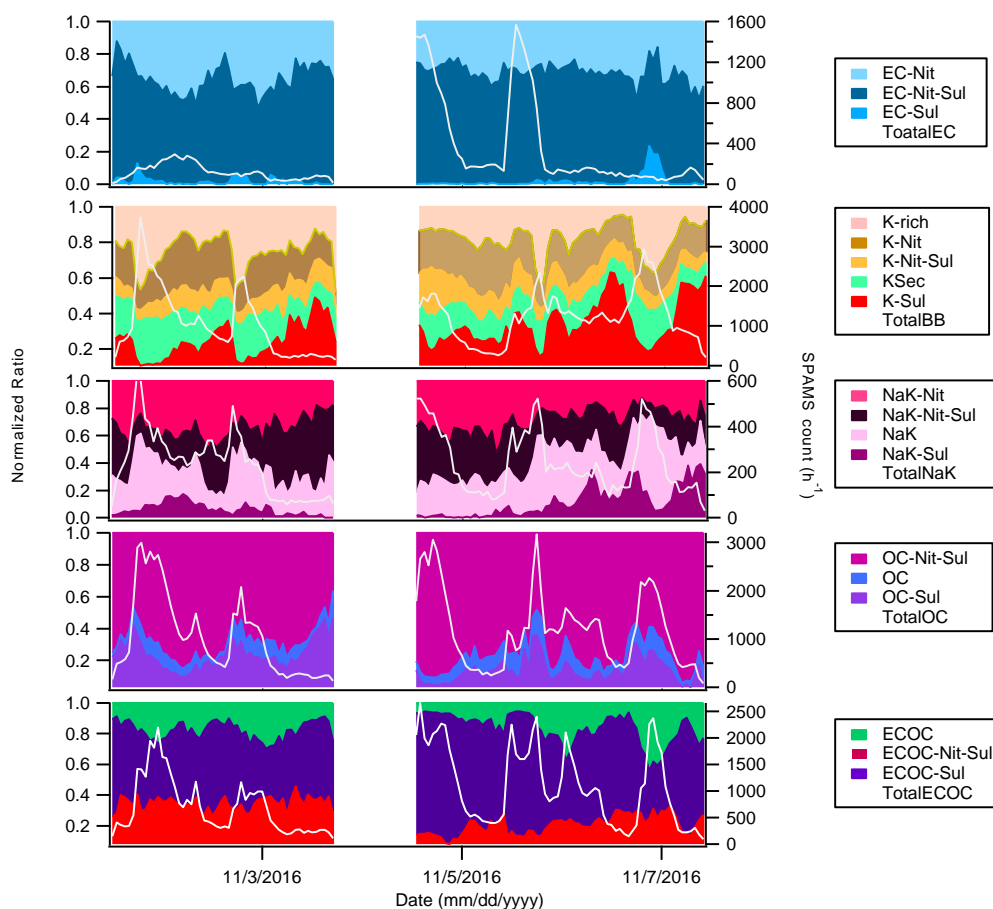
### 229 **3.5 Case studies: Haze events at PG**

230 A pollution event occurred at PG (E1\_PG) from 11/01 to 11/08. During this period, a  
231 similar pattern of transport and accumulation was also observed. At the beginning of each  
232 pollution event, there was also a transport process of particles from the southwest (Figure  
233 3); when the wind speed reached  $< 2 \text{ m s}^{-1}$ , accumulations began, and the haze dispersed  
234 with the elevating wind speed. The development of haze events was similar, and Figure 3  
235 lists all the favorable wind directions for transport with red rectangles. As shown in Figure  
236 8, EC-Nit and EC-Nit-Sul showed unclear diurnal patterns, indicating that both particle  
237 types were transported regionally. K-rich, NaK, OC, and ECOC had clear diurnal heating  
238 and cooking patterns, suggesting that local sources were dominant. Such aged particle  
239 types as OC-Nit-Sul and ECOC-Nit-Sul increased due to local aging processes during  
240 E1\_PG. Therefore, E1\_PG was mainly driven by the input of particles, local emissions,  
241 and accumulation. Moreover, the relative abundance of ECOC-Nit-Sul increased twofold  
242 from 2:00 on 11/03/2016 to 12:00 on 11/03/2016, suggesting the contribution of secondary  
243 formation (Figure 8).

244 When E4\_PG occurred, transport from the southwest was identified along with the  
245 transport of EC-Sul and EC-Nit-Sul, resulting in a  $\text{PM}_{2.5}$  concentration of  $176 \mu\text{g m}^{-3}$  at  
246 10:00 on 11/24/2016. The average wind speed was  $1.5 \text{ ms}^{-1}$  at the time, representing a  
247 typical stagnant-air condition. All particle families showed accumulation trends after that  
248 (Figure 3). The sharp decrease of all particle families was due to the high western wind  
249 speed ( $> 4 \text{ ms}^{-1}$ ) at 12:00 on 11/26/2016. During particulate accumulation at PG, such local  
250 particle types as ECOC, OC, and NaK still had diurnal patterns, but the aged “-Nit-Sul”

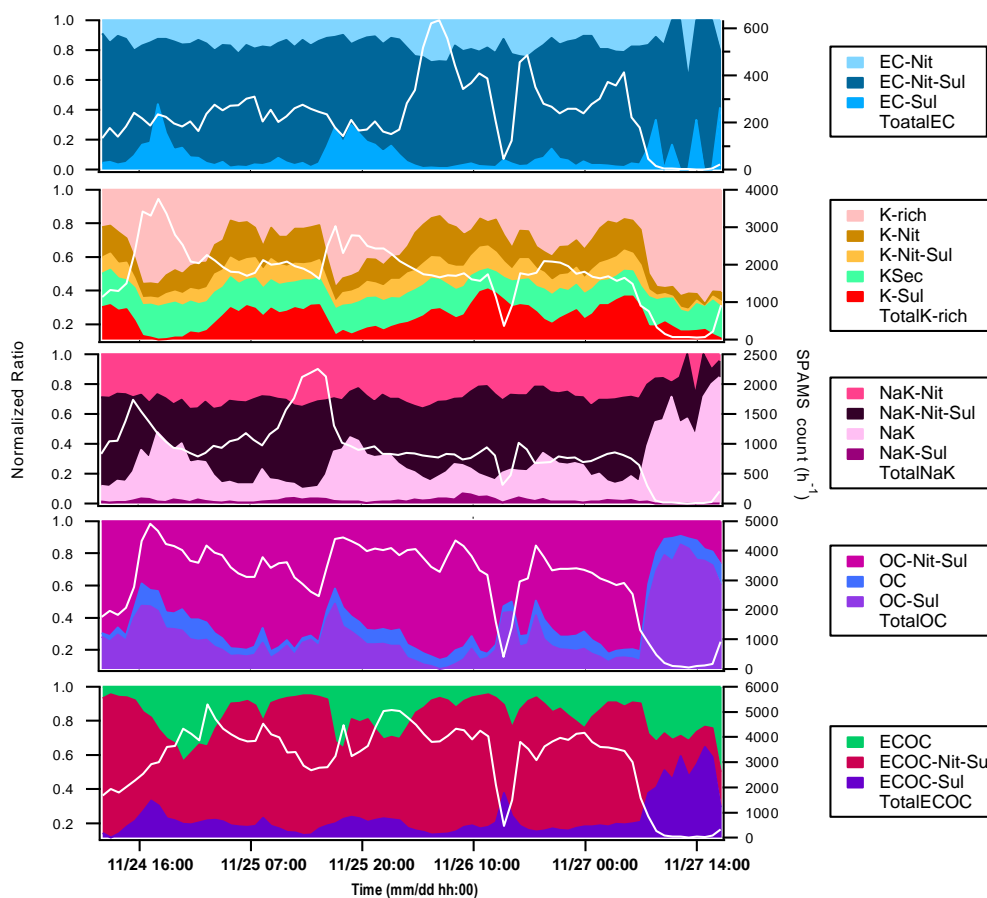


251 particles types were predominant (> 50% in all particle families). Thus, the local  
252 accumulation of pollutants was the major driver of E4\_PG (Figure 8).



253

254 Figure 7. Time trends of number ratios of particle types (left) and hourly counts of particle  
255 families (EC, BB, NaK, OC, and ECOC, right) during Pollution Event 1 (E1 11/01–11/08)  
256 at PG.



257

258 Figure 8. Time trends of number ratios of particle types (left) and hourly counts of particle  
259 families (EC, BB, NaK, OC, and ECOC, right) during Pollution Event 4 (E4) at PG.

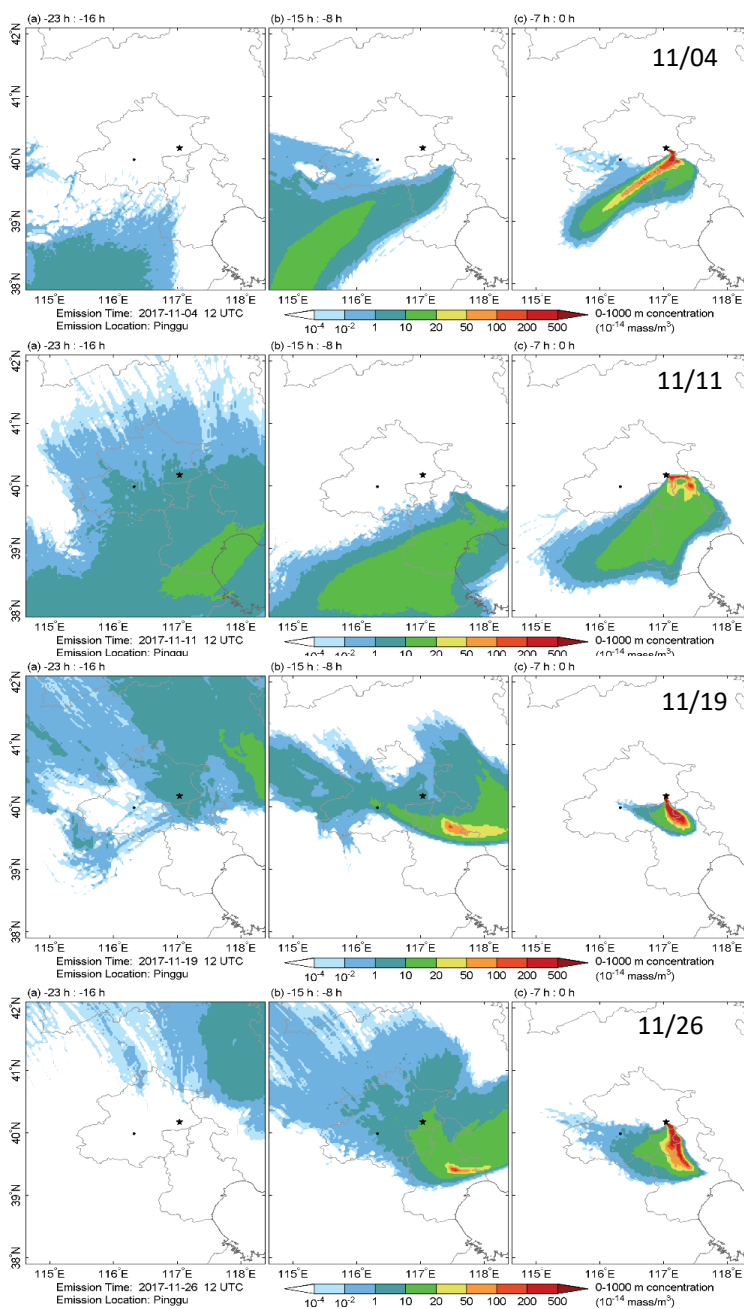
### 260 3.6 Interaction of PM between PKU and PG

261 Since PKU and PG share 17 common particle types, possible transport between the two  
262 sites was validated using the HYSPLIT model. All cases of transport are available in  
263 Supplementary information (Figures S11 and S12). Figures 9 and 10 only illustrate the  
264 examples of transport during each pollution event. The PKU site is located on the edge of  
265 plumes originating from PG during E1, which implies that the particulate transport was



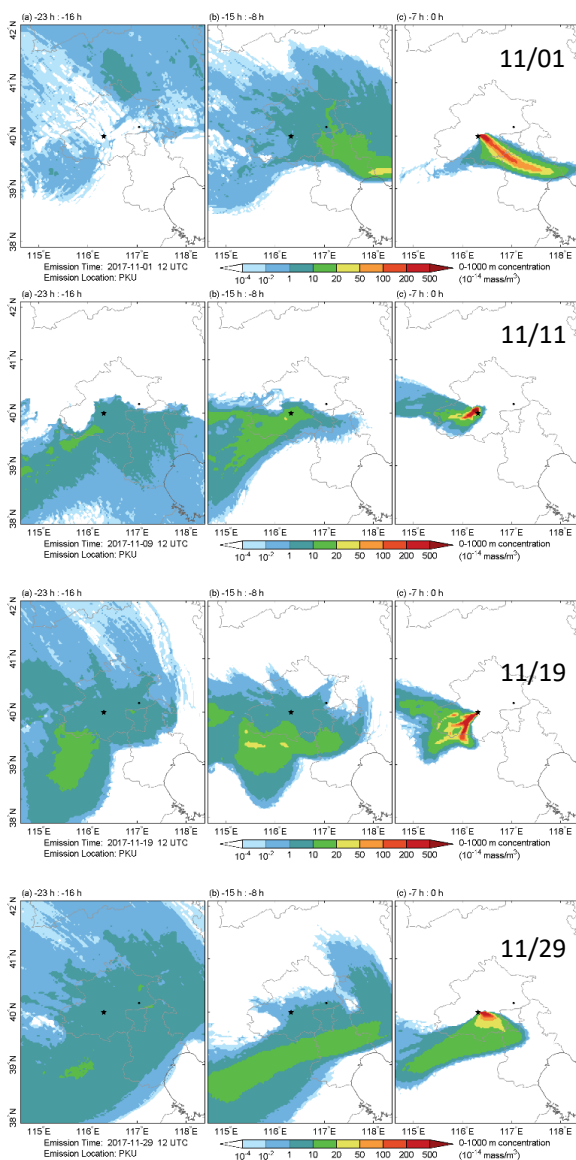
266 partially from PG (Figure 9). Moreover, the PKU site lies in the high concentration zone  
267 of plumes PG from during E3 and E4. Therefore, E3\_PKU and E4\_PKU were confidently  
268 considered input haze events. In contrast, the relatively slighter transport of air mass from  
269 PKU to PG was observed during these events. As shown in Figure 10, the air mass passing  
270 through the PKU site mainly influenced the areas in the south and east. Consequently, the  
271 PG site was seldom in the high concentration zone of plumes originating from PKU.

272 Figures 9 and 10 suggest that pollutants were transported significantly from PG to PKU  
273 during stagnant air conditions when dense haze occurred. These results are consistent with  
274 the analysis of particle categories. In an urban area such as PKU, the local EC particles  
275 were associated with the ECOC and OC families causing severe pollution in the urban area.  
276 On the other hand, in the rural area, the aged particles were dominant under stagnant air  
277 conditions and transported to PKU, leading to extreme urban particulate pollution. Besides,  
278 our results are consistent with other studies in the APHH-Beijing Project. For example, Du  
279 et al. (2019) have confirmed that regional transport plays a non-negligible role in haze  
280 episodes with contributions of 14–31% to the surface PM<sub>2.5</sub> mass concentration.



281

282 Figure 9. Typical dispersion of air mass from PG (star, on the right) to PKU (dot, on the  
283 left) during E1 (11/04), E2 (11/11), E3 (11/19) and E4 (11/26).



284

285 Figure 10. Typical dispersion of air mass from PKU (star, on the left) to PG (dot, on the  
286 right) in E1 (11/01), E2 (11/11), E3 (11/19) and E4 (11/29).

287



### 288 **3.7 Implications**

289 This study provides the polar plots that are used to explain the interaction of pollutants and  
290 wind. Such regional pollution sources as BB and the coal and steel industries have a strong  
291 impact on the particulate chemical composition of the air in urban Beijing. Besides,  
292 according to model studies, air pollutants in such provinces as Hebei, Henan, and Shandong  
293 are transported to Beijing (Shi et al., 2019; Du et al., 2019). In these provinces, efforts have  
294 been made to abate emissions from the steel industry, power plants, and traffic. However,  
295 BB accounted for 10–20% of the PM<sub>2.5</sub> in the study period (Liu et al., 2019). In particular,  
296 household biofuel combustion is a primary BB source during winter, impacting both  
297 outdoor and indoor air quality (Zhang and Cao, 2015). Therefore, more attention should be  
298 paid to tackling BB emissions.

299 This study improves our general understanding of the sources of sulfates in Beijing.  
300 Particles that only increased with the uptake of sulfate, such as OC-Sul\_PKU, K-Sul\_PKU,  
301 and NaK-Sul\_PKU, were transported regionally and arrived at the sampling site during  
302 high wind speeds ( $> 4 \text{ m s}^{-1}$ ). The results are consistent with the findings of Duan et al.  
303 (2019) that sulfates in Beijing during winter are formed regionally. Nitrate-containing  
304 particles could be found after processing in the NO<sub>x</sub>-rich urban and rural plumes of Beijing.  
305 Since SPAMS is limited in tracking such partial organics as hydrocarbons and PAHs, the  
306 evolution of secondary organics is unavailable in this study.

307 Just as Zhong et al. (2017) reported, this study found that there was a process of particle  
308 transport before severe haze events began in Beijing. However, there are still unresolved  
309 issues regarding the causal relationship between particle transport and haze events. There  
310 are two possibilities. The first is that transported PM<sub>2.5</sub> can trigger an anomalous inversion



311 before a pollution event, resulting in unfavorable meteorological conditions. The second is  
312 that transportation is a consequence of weakening atmospheric circulation causing air  
313 stagnation. In a most recent study of aerosol–radiation feedback deterioration in Beijing  
314 during wintertime, Wu et al. (2019) have proposed that the increase of near-surface PM<sub>2.5</sub>  
315 from 10 to 200  $\mu\text{g m}^{-3}$  can result in a decreasing of planetary boundary layer (PBL) from  
316 1500 m to 400 m, consequently contributing the PM<sub>2.5</sub> concentration by 20%. They also  
317 proposed that the wind speed decreased by 0.2  $\text{m s}^{-1}$  when the PM<sub>2.5</sub> loading increase from  
318 10 to 200  $\text{m s}^{-1}$ . Therefore, the southerly transported particles were impossible to trigger  
319 severe haze pollution due to air stagnation; the particles from both southerly transport and  
320 accumulation were due to the attenuated near-surface atmospheric circulation.

#### 321 **4. Summary**

322 The wintertime haze events that occurred in Beijing from 11/01/2016 to 11/29/2016 have  
323 been investigated. The heating period, including central and residential heating in both  
324 urban and rural areas, severely impacted the particulate chemical composition in the region.  
325 In Beijing, a pattern of the transport and accumulation of particles was found in both the  
326 urban and rural areas. The input of regional particles was a consequence of weakening  
327 atmospheric circulations, resulting in the stagnation of the air which provided favorable  
328 conditions for the accumulation of pollutants, ultimately leading to severe haze events. In  
329 the rural area, the heavy haze was mainly controlled by air stagnation and local emissions,  
330 but regional transport was also observed before the event. We also discussed the influence  
331 of regional transport using the dispersion model. The air masses between PKU and PG  
332 interacted with each other whenever heavy haze occurred. Parts I and II of this study are



333 useful for understanding the formation mechanism of winter haze in both the urban and  
334 rural areas of Beijing. This study also implies that the mitigation of PM relies on both urban  
335 and rural areas.

336 *Data availability.* All the data described in this study is available upon request from the  
337 corresponding authors.

338 *Author contributions.* FY, MZ, TZ, and KH designed the experiments; YC, JC, ZW, MT,  
339 CP, and HY carried them out; XY, GS, and SZ analyzed the experimental data; YC  
340 prepared the manuscript with contributions from all coauthors.

341 *Competing interests.* The authors declare that they have no conflicts of interest.

342 *Acknowledgments.* We are grateful for financial support from the National Natural Science  
343 Foundation of China (Grant No. 41703136 and 81571130100).

344



345 References

- 346 Chagger, H., Jones, J., Pourkashanian, M., Williams, A., Owen, A., and Fynes, G.:  
347 Emission of volatile organic compounds from coal combustion, *Fuel*, 78, 1527-1538, 1999.
- 348 Che, H., Xia, X., Zhu, J., Li, Z., Dubovik, O., Holben, B., Goloub, P., Chen, H., Estelles,  
349 V., Cuevas-Agulló, E., Blarel, L., Wang, H., Zhao, H., Zhang, X., Wang, Y., Sun, J., Tao,  
350 R., and Shi, G.: Column aerosol optical properties and aerosol radiative forcing during a  
351 serious haze-fog month over North China Plain in 2013 based on ground-based  
352 sunphotometer measurements, *Atmos. Chem. Phys.*, 14, 2125-2138, 10.5194/acp-14-2125-  
353 2014, 2014.
- 354 Chen, Q. C., Sun, H.Y., Mu, Z., Wang, Y.Q., Li, Y.G., Zhang, L.X., Wang, M.M., Zhang,  
355 Z.M.: Characteristics of environmentally persistent free radicals in PM<sub>2.5</sub>: Concentrations,  
356 species and sources in Xi'an, Northwestern China\*, *Environ Pollut*, 247, 18-26,  
357 10.1016/j.envpol.2019.01.015., 2019.
- 358 Chen, Y., Ebenstein, A., Greenstone, M., and Li, H.: Evidence on the impact of sustained  
359 exposure to air pollution on life expectancy from China's Huai River policy, *Proceedings*  
360 *of the National Academy of Sciences*, 110, 12936-12941, 2013.
- 361 Chen, Y., Cao, J., Huang, R., Yang, F., Wang, Q., and Wang, Y.: Characterization, mixing  
362 state, and evolution of urban single particles in Xi'an (China) during wintertime haze days,  
363 *Sci. Total Environ.*, 573, 937-945, 10.1016/j.scitotenv.2016.08.151, 2016a.
- 364 Chen, Y., Schleicher, N., Fricker, M., Cen, K., Liu, X. L., Kaminski, U., Yu, Y., Wu, X.  
365 F., and Norra, S.: Long-term variation of black carbon and PM<sub>2.5</sub> in Beijing, China with



- 366 respect to meteorological conditions and governmental measures, *Environ. Pollut.*, 212,  
367 269-278, 10.1016/j.envpol.2016.01.008, 2016b.
- 368 Chen, Y., Cai, J., Wang, Z., Peng, C., Yao, X., Tian, M., Han, Y., Shi, G., Shi, Z., Liu, Y.,  
369 Yang, X., Zheng, M., Zhu, T., He, K., Zhang, Q., and Yang, F.: Simultaneous Measurement  
370 of Urban and Rural Single Particles in Beijing, Part I: Chemical Composition and Mixing  
371 State, *Atmos. Chem. Phys. Discuss.*, 2020, 1-40, 10.5194/acp-2019-933, 2020.
- 372 Cheng, Y., Zheng, G., Wei, C., Mu, Q., Zheng, B., Wang, Z., Gao, M., Zhang, Q., He, K.,  
373 and Carmichael, G.: Reactive nitrogen chemistry in aerosol water as a source of sulfate  
374 during haze events in China, *Science Advances*, 2, e1601530, 2016.
- 375 Du, H., Li, J., Chen, X., Wang, Z., Sun, Y., Fu, P., Li, J., Gao, J., and Wei, Y.: Modeling  
376 of aerosol property evolution during winter haze episodes over a megacity cluster in  
377 northern China: roles of regional transport and heterogeneous reactions of SO<sub>2</sub>, *Atmos.*  
378 *Chem. Phys.*, 19, 9351-9370, 10.5194/acp-19-9351-2019, 2019.
- 379 Duan, J., Huang, R. J., Lin, C., Dai, W., Wang, M., Gu, Y., Wang, Y., Zhong, H., Zheng,  
380 Y., Ni, H., Dusek, U., Chen, Y., Li, Y., Chen, Q., Worsnop, D. R., O'Dowd, C. D., and  
381 Cao, J.: Distinctions in source regions and formation mechanisms of secondary aerosol in  
382 Beijing from summer to winter, *Atmos. Chem. Phys.*, 19, 10319-10334, 10.5194/acp-19-  
383 10319-2019, 2019.
- 384 Guo, S., Hu, M., Zamora, M. L., Peng, J., Shang, D., Zheng, J., Du, Z., Wu, Z., Shao, M.,  
385 Zeng, L., Molina, M. J., and Zhang, R.: Elucidating severe urban haze formation in China,  
386 *Proc Natl Acad Sci U S A*, 111, 17373-17378, 10.1073/pnas.1419604111, 2014.



- 387 He, H., Tie, X., Zhang, Q., Liu, X., Gao, Q., Li, X., and Gao, Y.: Analysis of the causes of  
388 heavy aerosol pollution in Beijing, China: A case study with the WRF-Chem model,  
389 *Particuology*, 20, 32-40, 2015.
- 390 Lee, R. G., Coleman, P., Jones, J. L., Jones, K. C., and Lohmann, R.: Emission factors and  
391 importance of PCDD/Fs, PCBs, PCNs, PAHs and PM10 from the domestic burning of coal  
392 and wood in the UK, *Environ. Sci. Technol.*, 39, 1436-1447, 2005.
- 393 Li, L., Huang, Z., Dong, J., Li, M., Gao, W., Nian, H., Fu, Z., Zhang, G., Bi, X., Cheng, P.,  
394 and Zhou, Z.: Real time bipolar time-of-flight mass spectrometer for analyzing single  
395 aerosol particles, *Int. J. Mass spectrom.*, 303, 118-124, 10.1016/j.ijms.2011.01.017, 2011.
- 396 Li, P., Yan, R., Yu, S., Wang, S., Liu, W., and Bao, H.: Reinstatement regional transport of  
397 PM<sub>2.5</sub> as a major cause of severe haze in Beijing, *Proc Natl Acad Sci U S A*, 112, 2015.
- 398 Linak, W. P., Yoo, J.-I., Wasson, S. J., Zhu, W., Wendt, J. O. L., Huggins, F. E., Chen, Y.,  
399 Shah, N., Huffman, G. P., and Gilmour, M. I.: Ultrafine ash aerosols from coal combustion:  
400 Characterization and health effects, *Proceedings of the Combustion Institute*, 31, 1929-  
401 1937, 10.1016/j.proci.2006.08.086, 2007.
- 402 Liu, Y., Zheng, M., Yu, M., Cai, X., Du, H., Li, J., Zhou, T., Yan, C., Wang, X., Shi, Z.,  
403 Harrison, R. M., Zhang, Q., and He, K.: High-time-resolution source apportionment of  
404 PM<sub>2.5</sub> in Beijing with multiple models, *Atmos. Chem. Phys.*, 19,  
405 6595-6609, 10.5194/acp-19-6595-2019, 2019.
- 406 Ma, L., Li, M., Huang, Z., Li, L., Gao, W., Nian, H., Zou, L., Fu, Z., Gao, J., Chai, F., and  
407 Zhou, Z.: Real time analysis of lead-containing atmospheric particles in Beijing during



408 springtime by single particle aerosol mass spectrometry, *Chemosphere*, 154, 454-462,  
409 10.1016/j.chemosphere.2016.04.001, 2016.

410 Quan, J., Gao, Y., Zhang, Q., Tie, X., Cao, J., Han, S., Meng, J., Chen, P., and Zhao, D.:  
411 Evolution of planetary boundary layer under different weather conditions, and its impact  
412 on aerosol concentrations, *Particuology*, 11, 34-40,  
413 <http://dx.doi.org/10.1016/j.partic.2012.04.005>, 2013.

414 Shi, Z., Vu, T., Kotthaus, S., Harrison, R. M., Grimmond, S., Yue, S., Zhu, T., Lee, J., Han,  
415 Y., Demuzere, M., Dunmore, R. E., Ren, L., Liu, D., Wang, Y., Wild, O., Allan, J., Acton,  
416 W. J., Barlow, J., Barratt, B., Beddows, D., Bloss, W. J., Calzolari, G., Carruthers, D.,  
417 Carslaw, D. C., Chan, Q., Chatzidiakou, L., Chen, Y., Crilley, L., Coe, H., Dai, T., Doherty,  
418 R., Duan, F., Fu, P., Ge, B., Ge, M., Guan, D., Hamilton, J. F., He, K., Heal, M., Heard,  
419 D., Hewitt, C. N., Hollaway, M., Hu, M., Ji, D., Jiang, X., Jones, R., Kalberer, M., Kelly,  
420 F. J., Kramer, L., Langford, B., Lin, C., Lewis, A. C., Li, J., Li, W., Liu, H., Liu, J., Loh,  
421 M., Lu, K., Lucarelli, F., Mann, G., McFiggans, G., Miller, M. R., Mills, G., Monk, P.,  
422 Nemitz, E., O'Connor, F., Ouyang, B., Palmer, P. I., Percival, C., Popoola, O., Reeves, C.,  
423 Rickard, A. R., Shao, L., Shi, G., Spracklen, D., Stevenson, D., Sun, Y., Sun, Z., Tao, S.,  
424 Tong, S., Wang, Q., Wang, W., Wang, X., Wang, X., Wang, Z., Wei, L., Whalley, L., Wu,  
425 X., Wu, Z., Xie, P., Yang, F., Zhang, Q., Zhang, Y., Zhang, Y., and Zheng, M.: Introduction  
426 to the special issue “In-depth study of air pollution sources and processes within Beijing  
427 and its surrounding region (APHH-Beijing)”, *Atmos. Chem. Phys.*, 19, 7519-7546,  
428 10.5194/acp-19-7519-2019, 2019.



- 429 Sun, Y., Wang, Z., Fu, P., Jiang, Q., Yang, T., Li, J., and Ge, X.: The impact of relative  
430 humidity on aerosol composition and evolution processes during wintertime in Beijing,  
431 China, *Atmos. Environ.*, 77, 927-934, 10.1016/j.atmosenv.2013.06.019, 2013a.
- 432 Sun, Y., Wang, Z., Fu, P., Yang, T., Jiang, Q., Dong, H., Li, J., and Jia, J.: Aerosol  
433 composition, sources and processes during wintertime in Beijing, China, *Atmos. Chem.*  
434 *Phys.*, 13, 4577-4592, 2013b.
- 435 Sun, Y., Jiang, Q., Wang, Z., Fu, P., Li, J., Yang, T., and Yin, Y.: Investigation of the  
436 sources and evolution processes of severe haze pollution in Beijing in January 2013,  
437 *Journal of Geophysical Research: Atmospheres*, 119, 4380-4398,  
438 doi:10.1002/2014JD021641, 2014.
- 439 Tian, S., Pan, Y., Liu, Z., Wen, T., and Wang, Y.: Size-resolved aerosol chemical analysis  
440 of extreme haze pollution events during early 2013 in urban Beijing, China, *J Hazard Mater*,  
441 279, 452-460, 2014.
- 442 Wang, G., Zhang, R., Gomez, M. E., Yang, L., Zamora, M. L., Hu, M., Lin, Y., Peng, J.,  
443 Guo, S., and Meng, J.: Persistent sulfate formation from London Fog to Chinese haze,  
444 *Proceedings of the National Academy of Sciences*, 113, 13630-13635, 2016.
- 445 Wang, J., Liu, D., Ge, X., Wu, Y., Shen, F., Chen, M., Zhao, J., Xie, C., Wang, Q., Xu, W.,  
446 Zhang, J., Hu, J., Allan, J., Joshi, R., Fu, P., Coe, H., and Sun, Y.: Characterization of black  
447 carbon-containing fine particles in Beijing during wintertime, *Atmos. Chem. Phys.*, 19,  
448 447-458, 10.5194/acp-19-447-2019, 2019.
- 449 Wu, J., Bei, N., Hu, B., Liu, S., Zhou, M., Wang, Q., Li, X., Liu, L., Feng, T., Liu, Z.,  
450 Wang, Y., Cao, J., Tie, X., Wang, J., Molina, L. T., and Li, G.: Aerosol–radiation feedback



451 deteriorates the wintertime haze in the North China Plain, *Atmos. Chem. Phys.*, 19, 8703-  
452 8719, [10.5194/acp-19-8703-2019](https://doi.org/10.5194/acp-19-8703-2019), 2019.

453 Xu, J., Wang, H., Li, X., Li, Y., Wen, J., Zhang, J., Shi, X., Li, M., Wang, W., Shi, G., and  
454 Feng, Y.: Refined source apportionment of coal combustion sources by using single  
455 particle mass spectrometry, *Sci. Total Environ.*, 627, 633-646,  
456 <https://doi.org/10.1016/j.scitotenv.2018.01.269>, 2018a.

457 Xu, J., Wang, H., Li, X., Li, Y., Wen, J., Zhang, J., Shi, X., Li, M., Wang, W., Shi, G., and  
458 Feng, Y.: Refined source apportionment of coal combustion sources by using single  
459 particle mass spectrometry, *Sci. Total Environ.*, 627, 633-646,  
460 [10.1016/j.scitotenv.2018.01.269](https://doi.org/10.1016/j.scitotenv.2018.01.269), 2018b.

461 Zhang, J., Huang, X., Chen, Y., Luo, B., Luo, J., Zhang, W., Rao, Z., and Yang, F.:  
462 Characterization of lead-containing atmospheric particles in a typical basin city of China:  
463 Seasonal variations, potential source areas, and responses to fireworks, *Sci. Total Environ.*,  
464 661, 354-363, <https://doi.org/10.1016/j.scitotenv.2019.01.079>, 2019.

465 Zhang, L., Wang, T., Lv, M., and Zhang, Q.: On the severe haze in Beijing during January  
466 2013: Unraveling the effects of meteorological anomalies with WRF-Chem, *Atmos.*  
467 *Environ.*, 104, 11-21, <https://doi.org/10.1016/j.atmosenv.2015.01.001>, 2015.

468 Zhang, Y.-L., and Cao, F.: Is it time to tackle PM<sub>2.5</sub> air pollutions in China from biomass-  
469 burning emissions?, *Environ. Pollut.*, 202, 217-219,  
470 [http://dx.doi.org/10.1016/j.envpol.2015.02.005](https://doi.org/10.1016/j.envpol.2015.02.005), 2015.



471 Zhang, Y., Chen, J., Yang, H., Li, R., and Yu, Q.: Seasonal variation and potential source  
472 regions of PM<sub>2.5</sub>-bound PAHs in the megacity Beijing, China: Impact of regional transport,  
473 Environ. Pollut., 231, 329-338, 10.1016/j.envpol.2017.08.025, 2017.

474 Zhong, J., Zhang, X., Wang, Y., Sun, J., Zhang, Y., Wang, J., Tan, K., Shen, X., Che, H.,  
475 Zhang, L., Zhang, Z., Qi, X., Zhao, H., Ren, S., and Li, Y.: Relative contributions of  
476 boundary-layer meteorological factors to the explosive growth of PM<sub>2.5</sub> during the red-  
477 alert heavy pollution episodes in Beijing in December 2016, Journal of Meteorological  
478 Research, 31, 809-819, 10.1007/s13351-017-7088-0, 2017.

479